An evaluation of the synergy of satellite passive microwave observations between 1.4 and 36 GHz, for vegetation characterization over the Tropics

Catherine Prigent, Carlos Jimenez

An evaluation of the synergy of satellite passive microwave observations between 1.4 and 36 GHz, for vegetation characterization over the Tropics

published in Remote Sensing of Environment

Catherine Prigent and Carlos Jimenez,
CNRS, Paris Observatory, France.
Estellus, Paris, France.

Abstract

Satellite passive microwave observations from 1.4 to 36 GHz already showed sensitivity to vegetation parameters, primarily through the calculations of the Vegetation Optical Depth (VOD) at individual window frequencies, separately. Here we evaluate the synergy of this frequency range for vegetation characterization, through the estimation of two vegetation parameters, its foliage and the photosynthesis activity as described by the Normalized Difference Vegetation Index (NDVI), and its woody components and carbon stock as described by the Above Ground Carbon (AGC), using different combinations of channels in the considered frequency range. Neural network retrievals are trained on these two vegetation parameters (NDVI and AGC), for several microwave channel combinations, including the future Copernicus Imaging Microwave Radiometer (CIMR) that will observe simultaneously in window channels from 1.4 to 36 GHz, for the first time. This methodology avoids the use of any assumptions in the complex interaction between the surface (vegetation and soil) and the radiation, as well as any ancillary observations, to propose a genuine and objective evaluation of the information content of the passive microwave frequencies for vegetation characterization. Our analysis quantifies the synergy of the microwave frequencies from 1.4 to 36 GHz, and shows the expected potential of the CIMR instrument for the monitoring of vegetation parameters in tropical environments, as compared to current instruments. It also confirms that the 1.4 GHz observations have

a high sensitivity to AGC, as compared to the other single frequencies up to 36 GHz, at least under tropical environments.

1 Introduction

Vegetation distribution and its dynamics strongly affect the Earth water, energy, and carbon cycles, through complex biogeophysical and biogeochemical processes, at intricate time and spatial scales [Bonan, 2015]. Vegetation covers ∼20% of the globe, and large scale monitoring of its parameters is critical, to evaluate its response to anthropogenic pressure and climate changes.

Satellite observations provide a unique possibility to monitor the vegetation distribution and dynamics at global scales on a regular basis. Vegetation monitoring from satellites has been primarily based on visible-infrared observations, with the Normalized Difference Vegetation Index (NDVI) being one of the most popular satellite-derived environmental parameters, available for ∼4 decades with kilometric spatial resolution (see [Tucker, 1979] for pioneering work). NDVI is calculated from the difference in the reflectances of green vegetation between red and near-infrared wavelengths and is representative of the amount of photosynthetically active chlorophyll components of the vegetation. Different parameters such as the Leaf Area Index (LAI) or the Fraction of Absorbed Photosynthetically Active Radiation (FAPAR) have been calculated using similar observations to characterize the green elements of the vegetation. However, NDVI being derived from visible and infrared observations, it is not available, or is at least contaminated, under cloudy conditions. In addition, it tends to saturate for dense vegetation such as tropical forests, as it is only representative of the top layer of the vegetation. Nevertheless, the visible-infrared observations (along with all its derived vegetation metrics) remain a very valuable source of information for vegetation studies, at local to global scales, for multiple applications (e.g., agriculture, weather prediction, climate monitoring).

Microwave satellite remote sensing offers complementary information on the vegetation [Chukhlantsev, 2006]. First, it is partly insensitive to clouds and it can sense within or below the vegetation canopy with lower frequencies having a greater penetration depth. Second, microwave observations are primarily sensitive to the water presence in the vegetation. Water strongly affects the dielectric properties of the media, modifying the attenuation, emission, and scattering of vegetation and soil at microwave frequencies [Ulaby et al., 1981, Ulaby and Long, 2015]. As a consequence, contrarily to visible-infrared information, the microwave observations should be rep-

resentative of both photosynthetic and non-photosynthetic above ground biomass, including trunk and branches. With increasing attenuation in the vegetation with increasing frequencies, it is expected that over a dense forest the lower microwave frequencies provide more information about the woody parts of the vegetation, whereas the higher microwave frequencies mostly sense the foliage in the canopy. Early works from [Choudhury et al., 1987, Paloscia and Pampaloni, 1988] showed evidence of a relationship between the passive microwave observations and the vegetation at large scales, followed by more quantitative assessments of vegetation properties (e.g., the vegetation biomass in [Wigneron et al., 1995], the vegetation water content in [Njoku and Li, 1999], or the vegetation phenology in [Shi et al., 2008]). The Vegetation Optical Depth (VOD) calculated from passive microwave observations (e.g., [Owe et al., 2001, Liu et al., 2011, Jones et al., 2011, Konings et al., 2016, Fernandez-Moran et al., 2017, Wigneron et al., 2021]) is typically based on the zeroth-order solution of the soil-vegetation radiative transfer equation (the tau-omega model), and it integrates the vegetation water content and structural effects. Several methods have been developed to calculate the VOD, using multi-polarizations, multi-angles, and/or multi-temporal observations depending on the possibilities offered by the instrument, with the help of ancillary data such as soil roughness, land surface temperature, and land cover classification (this later parameter possibly derived from NDVI-related products). See the review by [Frappart et al., 2020]. Recent developments in VOD calculation tend to limit the contribution of ancillary information for noise reduction, but still use some necessary external inputs [Fernandez-Moran et al., 2017, Wigneron et al., 2021]. Vegetation biomass estimation from microwaves assumes that the vegetation water content to which microwaves are sensitive is tightly linked to the biomass of the plant and to its carbon content, especially at low microwave frequencies that penetrate deep in the vegetation with less influence of green non-woody plant components [Liu et al., 2011, Brandt et al., 2018, Fan et al., 2019]. Benchmark forest carbon stocks have been mapped from the combination of in situ inventories and satellite data from lidar, from visible/infrared images, and from active microwave observations [Saatchi et al., 2011]. Significant correlation has been evidenced between the VOD at 1.4 GHz and large scale inventories of above ground carbon (for instance from [Saatchi et al., 2011]) and this relationship has been exploited to reveal recent carbon losses in African drylands [Brandt et al., 2018], or to quantify the inter-annual dynamics of the total tropical forest carbon [Fan et al., 2019]. VODs at higher frequencies have also been explored. For instance, [Jones et al., 2011, Jones et al., 2014] showed the sensitivity of the VOD at 10 and 18 GHz to the vegetation phe-

nology, overcoming limitations affecting satellite optical-infrared observations. Currently, the Soil Moisture and Ocean Salinity (SMOS) and the Soil Moisture Active Passive (SMAP) missions provide satellite observations at 1.4 GHz (L band), and measurements from 6 to 36 GHz (C, X, Ku, and Ka bands) are available from the Advanced Microwave Scanning Radiometer-2 (AMSR2).

The relative merit of passive microwave observations at different frequencies and their potential complementarity for vegetation characterization have been raised in several studies, from satellite observations (e.g., between 6 and 18 GHz [Njoku and Li, 1999], between 19 and 85 GHz [Prigent et al., 2001]) or from ground-based measurements (e.g., between 1.4 and 90 GHz [Calvet et al., 2010]). More recently, [Chaparro et al., 2019] compared the sensitivity of the VOD between 1.4 and 10 GHz to above ground carbon, as measured from airborne lidar in South American forests: although they showed that the 1.4 GHz band observations have a good potential for the quantification of the carbon stocks, they indicated the synergy of multi-frequency observations for an improved monitoring. [Baur et al., 2019] also analyzed VODs from 1.4 to 10 GHz, in an attempt to quantify the absorption and scattering losses as a function of vegetation type, and as a function of frequency. Their results showed that the VODs at 6 and 10 GHz are mostly sensitive to the leaf phenology, whereas the 1.4 GHz VOD variations are dominated by changes in the water content of stems and woody parts. [Li et al., 2021] inter-compared VOD at different frequencies, and showed that they have complementary capabilities in monitoring vegetation. All these studies suggest that the combined use of multiple microwave frequencies should allow new insights into the vegetation functioning.

The Copernicus Imaging Microwave Radiometer (CIMR) mission is currently being implemented by the European Space Agency (ESA) as a High Priority Expansion Mission. It partly inherits from previous studies conducted at ESA for the Multifrequency Imaging Microwave Radiometer (MIMR) [Bernard et al., 1990]. CIMR is a conically scanning microwave radiometer imager in a sun-synchronous polar orbit that will provide, for the first time, simultaneous measurements at 1.4, 6.9, 10.65, 18.7, and 36.5 GHz [Kilic et al., 2018]. With its large deployable $\sim$8 m antenna, it will have a spatial resolution of $\sim$55 km at 1.4 GHz, $\sim$15 km at 6 and 10 GHz, and $\sim$5 km at 18 and 36GHz. For an extensive description of the mission, see https://cimr.eu/sites/cimr.met.no/files/documents/CIMR-MRD-v2.0-20190305-ISSUED0.pdf. The potential synergy of the CIMR frequencies for the characterization of vegetation is expected, but still needs to be quantified at large scales.

Analyzing the synergy of the CIMR frequencies for vegetation characterization could be based on radiative transfer model simulations between 1.4 and 36 GHz, using a set of vegetation and soil input parameters. That would suppose the existence of a reliable and consistent radiative transfer model from 1.4 to 36 GHz, along with representative and coherent vegetation and soil parameters, at least at regional scales. [Njoku and Li, 1999] insisted on the difficulty to model the interaction between the microwave radiation and the land surface, due to the large number of factors that affect the emission and scattering processes (soil and vegetation numerous physical properties, surface temperature, atmosphere), to the non-linearity and complexity of the processes, to the spatial heterogeneity of the surface properties, and to the lack of in situ measurements with coincident observations to constrain the problem. Despite significant efforts in radiative transfer model developments, primarily at 1.4 GHz in the framework of SMOS and SMAP (e.g., [Ferrazzoli et al., 2002, Wigneron et al., 2007]), a recent evaluation of state-of-the-art radiative transfer models at 1.4 GHz at ECMWF still shows discrepancies with satellite observations [de Rosnay et al., 2020]. At higher frequencies, the simulation results are not expected to be better: insuring a consistent agreement between radiative transfer simulations and observations over a large frequency range is usually very challenging, as most models are partly based on ad hoc parameterization for specific instrument observing conditions (such as frequency, polarization, incidence angle). As discussed in [Baur et al., 2019], the retrieval of VOD from radiative transfer modeling often relies upon the assumption that several parameters, such as the effective physical temperature, the soil moisture at the penetration depth, or the effective surface roughness, are independent of the frequency, which is questionable when calculating the VODs at different frequencies, especially with the intent of comparing their potential. Exploiting the direct relationship between the satellite brightness temperatures and the geophysical variables is another solution that already proved efficient. For exemple for the estimation of soil moisture from passive microwave observations, a statistical neural network inverse model can be trained on coincident satellite observations and soil moisture model outputs at global scale [Aires et al., 2005, Kolassa et al., 2013]. This methodology is currently applied at ECMWF for near-real time operational estimation of soil moisture with SMOS [Rodriguez-Fernandez et al., 2019].

Here we propose an objective and direct analysis of the sensitivity of existing close-to-CIMR passive microwave observations from 1.4 to 36 GHz to the vegetation information over the Tropics. It consists in studying the direct statistical relationships between the satellite observations and veg-

etation parameters, without relying on characterizing the vegetation and soil response by radiative transfer modeling. It involves an attempt to retrieve two complementary vegetation parameters from existing close-to-CIMR multi-frequency microwave observations, the first vegetation parameter mostly related to the foliage and the photosynthesis activity of the chlorophyll (NDVI), and the second vegetation parameter representative of the woody components and its carbon stock (the Above Ground Carbon (AGC) quantity estimated from [Saatchi et al., 2011]). Notice that at this stage, the goal is not to develop an optimal retrieval method, but to analyze the information content of the multi-frequency observations for vegetation characterization and to quantify their potential synergies.

The passive microwave satellite observations and the vegetation related datasets are presented in Section 1. The methodology is described in Section 2. The results are discussed in Section 3, first with a general analysis of the sensitivity of the passive microwave data to the vegetation parameters, and then with the inversion of the vegetation parameters with multi-frequency passive microwaves and the quantification of the frequency synergy. Section 4 concludes this study.

2 Data

A large dataset of passive microwave satellite observations has been collected, along with spatially and temporally coincident vegetation related parameters, derived from visible-infrared satellite observations (NDVI) and from maps of the Above Ground Biomass (AGB). Data have been systematically averaged over a 0.25°x0.25° regular grid. All data with daily or sub-daily variations have also been averaged on a 8-day period, following the temporal pattern selected by MODIS products. Data are prepared for 2015. With SMAP data starting in April, the analysis covers April to December 2015. The surface waters have been filtered out, following the monthly mean surface water extent at 0.25° resolution, available from the Global Inundation Extent from Multi-Satellite version 2 (GIEMS2) [Prigent et al., 2020].

One key vegetation-related data set (the AGB reference map from [Saatchi et al., 2011]) is essentially available over the tropical area. As a consequence, this first analysis concentrates on the tropical region, from 22°S to 22°N. It nevertheless includes a large variety of environments, from semi-arid vegetation to tropical forests.

2.1 Satellite passive microwaves

The passive microwave signals over vegetated land surfaces are the complex result of soil properties (e.g., humidity, roughness), vegetation characteristics (e.g., fractional coverage within the field-of-view, water content, foliage structure), surface temperature (Ts), and atmospheric contribution. The atmospheric contribution (water vapor, clouds, and rain) decreases with decreasing frequencies, with rather limited contribution at 10 GHz and below. The presence of vegetation generally increases the surface emissivity, especially the horizontal polarization, and it tends to depolarize the soil contribution that can be rather specular. To reduce the impact of the surface temperature in the microwave signatures, MicroWave Indices (MWI) have been used very early [Choudhury et al., 1987]. Here, we calculated it as: MWI=100* (TBV-TBH)/(TBV+TBH), where TBV and TBH are, respectively, the brightness temperatures at vertical and horizontal polarizations. A factor 100 is used in this study as the (TBV-TBH)/(TBV+TBH) ratio is usually lower than 0.05 over vegetation. Neglecting the atmospheric contribution, the microwave brightness temperature TB can be written as TB=emissivity*Ts, and MWI then corresponds to the ratio of the emissivity polarization difference normalized by its sum.

In this study, we used passive microwave observations between 1.4 and 36 GHz. Only passive microwave observations at night or early morning are used, to further reduce the impact of the Ts diurnal variations. We are fully aware that passive microwaves are not only sensitive to the vegetation properties, and that the variability of many other parameters affects the variables (such as the soil moisture or roughness, especially at low frequency under sparse vegetation). MWI (as well as the emissivity polarization difference) is expected to decrease with vegetation density increase; over bare soils, it increases with soil moistures increase and decreases with soil roughness increase [Ulaby and Long, 2015].

2.1.1 The 1.4 GHz observations (L band)

The SMAP satellite, launched at the end of January 2015 by NASA, is equipped with a real aperture antenna of 6 m to observe the Earth surface at 1.4 GHz with a fixed 40° incidence angle and a native spatial resolution of 36 km x 47 km [Entekhabi et al., 2014]. We use the L1B 36 km L-band brightness temperature at vertical and horizontal polarizations from SMAP (https://nsidc.org/data/SPL1BTB/versions/4, [Piepmeier et al., 2018]).

2.1.2 The 6 to 36 GHz observations (C, X, Ku, and Ka bands)

AMSR2, on board the Japanese JAXA GCOM-W1 mission, provides observations at frequencies between 6 and 89 GHz, in both vertical and horizontal polarizations, with an incidence angle of 55°. We explored the frequencies that are common to the CIMR project, i.e., the 6, 10, 18, and 36 GHz channels, with respective spatial resolutions of 48, 33, 18, and 9 km. The other channels are more affected by the atmosphere (at 23.8 and 89.0 GHz) or are rather redundant to already selected channels (i.e., at 7.3 GHz). The top of the atmosphere TBs are extracted from the JAXA data center (https://suzaku.eorc.jaxa.jp/GCOM_W/index.html). The level L3 product is used [Maeda et al., 2016], already projected on a 0.25°x0.25° regular grid.

2.2 Vegetation-related datasets

2.2.1 MODIS vegetation indices

MODIS vegetation indices are derived from 16-day composites of reflectances in the red, near-infrared, and blue wavelengths. Two major vegetation indices are provided from the atmospherically-corrected reflectances: NDVI, calculated as the difference of the red (645 nm) and near-infrared (858 nm) reflectances over their sum, and the Enhanced Vegetation Index (EVI) that also uses the reflectances in the blue (469 nm), to minimize canopy background variations and maintain sensitivity over dense vegetation conditions. See for instance [Huete et al., 2002] and the very abundant NDVI and EVI literature. MODIS instruments from both Terra and Aqua satellites are combined to permit a higher temporal resolution product, especially in areas strongly affected by cloud coverage.

Here, the MOD13C1 (from Terra) and MYD13C1 (from Aqua) L3 products are both used (https://lpdaac.usgs.gov/products/mod13c1v006/), to provide vegetation estimates every 8 days (16-day composites produced alternatively every 8 days from the two satellites). The initial 0.05° grid (∼5 km) are aggregated to the 0.25°x0.25° regular grid in this study, for comparison with the other data.

2.2.2 Above Ground Carbon stock

A reference map of total forest biomass in the tropical region has been produced by [Saatchi et al., 2011], based on field measurements, Geoscience Laser Altimeter System (GLAS) LIDAR data, and spatial imagery from visible-infrared and active microwave data. A large collection of calibra-

tion plots (∼500) in coincidence with GLAS measurements is first analyzed, and the result is spatially extrapolated with MODIS, SRTM (Shuttle Radar Topography Mission), and QuikSCAT images. The benchmark map illustrates regional patterns at 1 km spatial resolution and provides methodologically comparable estimates of biomass, representative of circa 2000. Once the total biomass is estimated, it is commonly admitted that the carbon stock corresponds to 50% of the total biomass (e.g., [Saatchi et al., 2011, Brandt et al., 2018]). [Brown and Lugo, 1982] presents significant results, and some discussion is proposed in [Elias and Potvin, 2003] for instance. Here, we will also adopt the 50% coefficient to convert the biomass into carbon stock.

For comparison purposes, the [Avitabile et al., 2016] biomass map at 1 km spatial resolution is also tested in this study. It was obtained by merging in situ data from forest plots, with the [Saatchi et al., 2011] and the [Baccini et al., 2012] maps, using machine-learning techniques. The merged dataset is representative of the 2000-2010 period.

2.2.3 Land cover dataset

GlobCover is an ESA initiative providing land cover maps derived from the 300 m MERIS sensor on board the ENVISAT satellite mission. It contains 22 land cover classes and is representative of December 2004 - June 2006. This land cover classification is adopted in this study: the initial high resolution product is aggregated onto the 0.25°x0.25° regular grid, by selecting the dominant land cover type.

3 Method

Contrarily to methods using radiative transfer modeling, a purely statistical analysis of the passive microwave observations was conducted, with no a priori assumptions about vegetation or soil characteristics that could interfere or bias the results.

First, the direct relationship between the passive microwave observations from 1.4 to 36 GHz and the two vegetation parameters (NDVI and AGC) were studied. The spatial correlations were analyzed, over the Tropics, for a given time of the year (June). Maps of the temporal correlations between the variables were then calculated over the full period covered by the dataset, over the same region. The variations of the microwave observations were also studied, per vegetation types and for different seasons.

Then, we analyzed the synergy of the multi-frequency microwave observations by testing a statistical retrieval of two complementary vegetation parameters, one representative of the foliage (NDVI) and one related to the carbon stock (AGC), for different combinations of the microwave frequencies. To conduct the retrieval tests, we propose an inversion method based on the direct statistical relationships between the satellite observations and the vegetation parameters to estimate, using artificial neural networks (NN). Compared to multilinear regressions, the NN can account for complex and non-linear relationships between the variables while maintaining the algorithm simple and quick to run. NN regressions have been successfully applied to many remote sensing problems (e.g., [Aires et al., 2001, Jimenez et al., 2009, Rodriguez-Fernandez et al., 2019]). Multi Layered Perceptron (MLP) models [Rumelhart et al., 1986] were adopted. A NN is defined by the number of input neurons (the satellite information used for the retrieval), the number of outputs (the vegetation parameter to estimate) and the number of neurons in a hidden layer to control the complexity of the NN model. The MLP weights are assigned by a Marquardt-Levenberg backpropagation algorithm [Hagan and Menhaj, 1994], with a validation method to monitor the evolution of the training error and avoid overfitting to the training data set. For each retrieval test, corresponding to a frequency combination and one of the two vegetation parameter, a new MLP of one input layer, one hidden layer with a sigmoidal activation function, and one output layer with a linear function was trained. The number of inputs depended upon the frequency selection. For each passive microwave frequency, two inputs are selected: the MWI and the TBH, as experiments demonstrated that the addition of the TBH to the MWI systematically improved the results.

Tests showed that one hidden layer with a sufficiently large number of neurons was sufficient. For a given output (NDVI or AGC), the NNs corresponding to the different frequency combinations were all trained on the same dataset, to insure fair comparisons. It corresponds to a subset of the initial dataset (one 8-day averaged period per season over a 9 month initial 8-day averaged dataset, i.e., $\sim$12% of the initial dataset), over the Tropical continental area (from 22°S to 22°N). Different training datasets were tested (more than one 8-day average per month, and changing the months), with very similar results. For NDVI, time coincident NDVI and passive microwave observations are considered. However, AGC from [Saatchi et al., 2011] being a static reference, the NNs to reproduce AGC are always trained on the same AGC values, regardless of the time period.

The retrievals were then tested on the original data set, excluding the data used to train the NNs. Two metrics assessed the quality of the re-

trievals: the coefficient of determination R^2 (the square of the linear correlation coefficient R), and the Root Mean Square Error ($RMSE$) calculated from the difference between the retrieved value and the truth. Note that the systematic error (or bias) is expected to be 0 over the full dataset, by construction of the NNs, and as a consequence, RMSE is very close to the random error for this dataset. Comparisons of the metrics for the retrievals using the different frequency combinations made it possible to quantify the synergy between the frequencies.

4 Results

4.1 Large Scale Correlation Analysis

Figure 1 presents images of MWI at 1.4 GHz from SMAP, and at 6 and 18 GHz from AMSR2 over the Tropics, for June 2015, along with corresponding the MODIS NDVI image. The static AGC [Saatchi et al., 2011] is also shown. MWI at 1.4 GHz shows a larger dynamical range than MWI at 6 or 18 GHz. This is particularly clear in the transition zone from the Sahara deserts southward to the equatorial forest in Africa or in South America, from the east to the west coast, along latitudes around 10°S. The tropical forest around the equator in Africa, indicated by high NDVI and high AGC, is well delineated at 1.4 GHz, with low MWI showing spatial patterns similar to NDVI and AGC.

To characterize the relationship between the passive microwave observations and the vegetation parameters, the density plots of selected pairs of variables are presented in Figure2, along with the corresponding coefficient of determination (R^2), first with NDVI, second with AGC, for the region (the Tropics) and month (June) displayed in Figure 1. The relationship between NDVI and EVI is also presented as well as the link between AGC from [Saatchi et al., 2011] and from [Avitabile et al., 2016]. Deserts (following the GlobCover classification) and surface waters (following a monthly climatology calculated from [Prigent et al., 2020]) are excluded from the analysis. R^2 between MWI and NDVI increases between 1.4 and 6 GHz, but then decreases from 6 to 18 GHz (with similar results at 18 and 36 GHz, not shown). Note that the scatterplot of MWI at 1.4 GHz versus NDVI presents two branches for the same high values of MWI: even with rather high density of green vegetation (rather high NDVI), observations at 1.4 GHz can detect the soil moisture and can present high polarization differences (high MWI). R^2 between MWI and AGC strongly decreases from 1.4 to 6 GHz and keeps decreasing to 18 GHz, with similar R^2 at 18 and 36 GHz (not

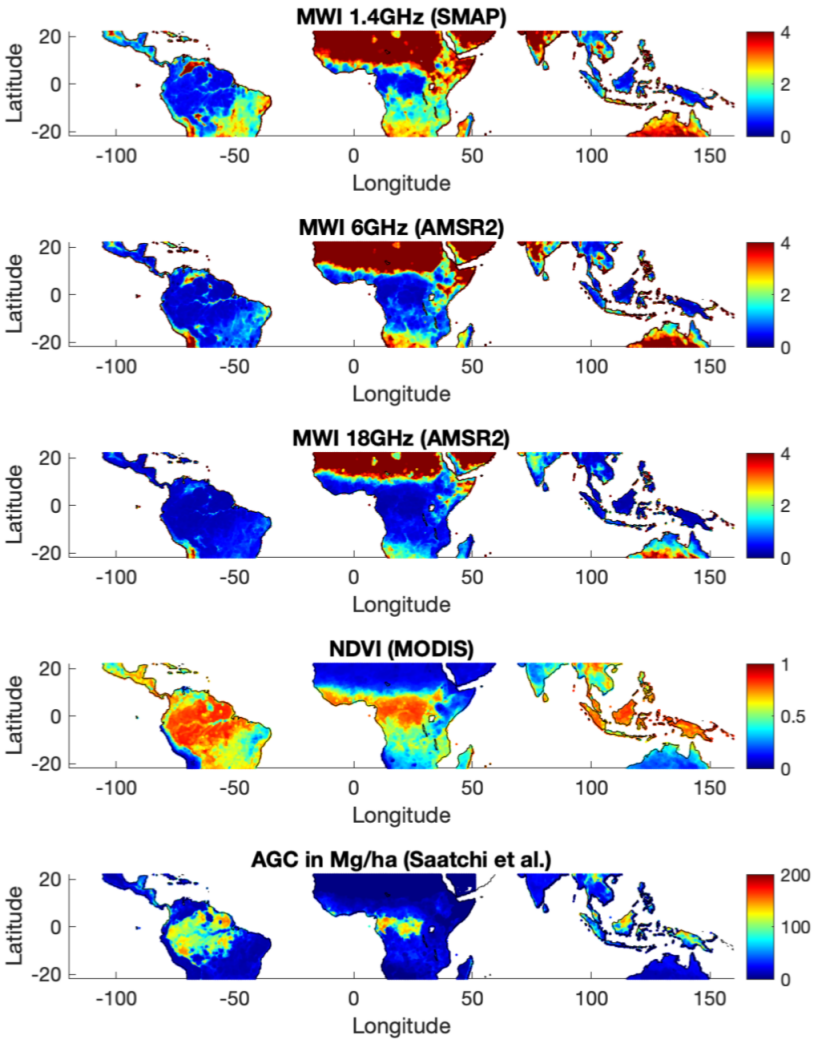

Figure 1: From top to bottom: the MicroWave Index (MWI) at 1.4 GHz (calculated from SMAP), at 6 and 18 GHz (calculated from AMSR2), the Normalized Difference Vegetation Index (NDVI) from MODIS, and the Above Ground Carbon (AGC) in Mg/ha from [Saatchi et al., 2011], for the Tropics, averaged over June 2015 for MWI and NDVI.

shown). The scatterplot of NDVI versus AGC shows that for low AGCs (<50 Mg/ha), the NDVI dynamics can be significant (from 0.1 to 0.8). This is likely representative of the photosynthesis activity of chlorophyll in rather low vegetation with limited trees (limited carbon content). For high NDVI (>0.75), AGC presents a rather large range of values that are expected to characterize a variety of dense forest areas with varying carbon contents. NDVI and EVI are strongly correlated (R^2=0.85) but the amplitude of variation for EVI is clearly smaller than for NDVI. Contrarily to what is sometimes shown, EVI here tends to saturate over very dense vegetation and rarely exceeds 0.5 even over tropical forests. We checked that the correlation coefficient is always smaller between MWI and EVI than between MWI and NDVI. [Saatchi et al., 2011] used NDVI and not EVI to interpolate the biomass information among in situ AGB estimates to produce their benchmark biomass map, as well as several other studies related to dense vegetation (e.g., [Brandt et al., 2018]). Our analysis here also tends to favor NDVI versus EVI, for the characterization of dense forests.

The previous analysis focused on the spatial correlations between the different variables for a given time of the year (June). The temporal correlations between NDVI and MWIs are presented in Figure 3 (statistical significance is tested, and pixels with p<0.05 are not displayed). It is calculated over April to December 2015, with SMAP not available before. The temporal correlations between NDVI and MWI at 1.4 GHz are dominantly positive, except in regions of very dense forests around the equator (where the correlation is negative or not statistically significant). For most locations, when NDVI increases, i.e., the 'green' vegetation grows, MWI at 1.4 GHz also increases, i.e., the emissivity polarization difference increases. 'Green' vegetation increases with available soil moisture for plant growth and correlation between NDVI and MWI is expected. The opposite prevails at 6 GHz and at higher frequencies (not shown), where negative correlations between NDVI and MWI time series are observed. The temporal correlations between MWI at 1.4 and 6 GHz are nevertheless mostly positive. The difference in behavior between 1.4 GHz and higher frequencies with respect to NDVI indicates some complementarity between the passive microwave frequencies that could be exploited, to better characterize the vegetation. The physical interpretation of these behaviors in the passive microwaves is due to different extinction in the vegetation as a function of frequency, related to both attenuation and scattering by the vegetation elements containing water. As already stressed by [Baur et al., 2019] or [Momen et al., 2017], the extinction is not only due to the absorption by the water in the vegetation, but also to the scattering of the microwave radiation by the canopy

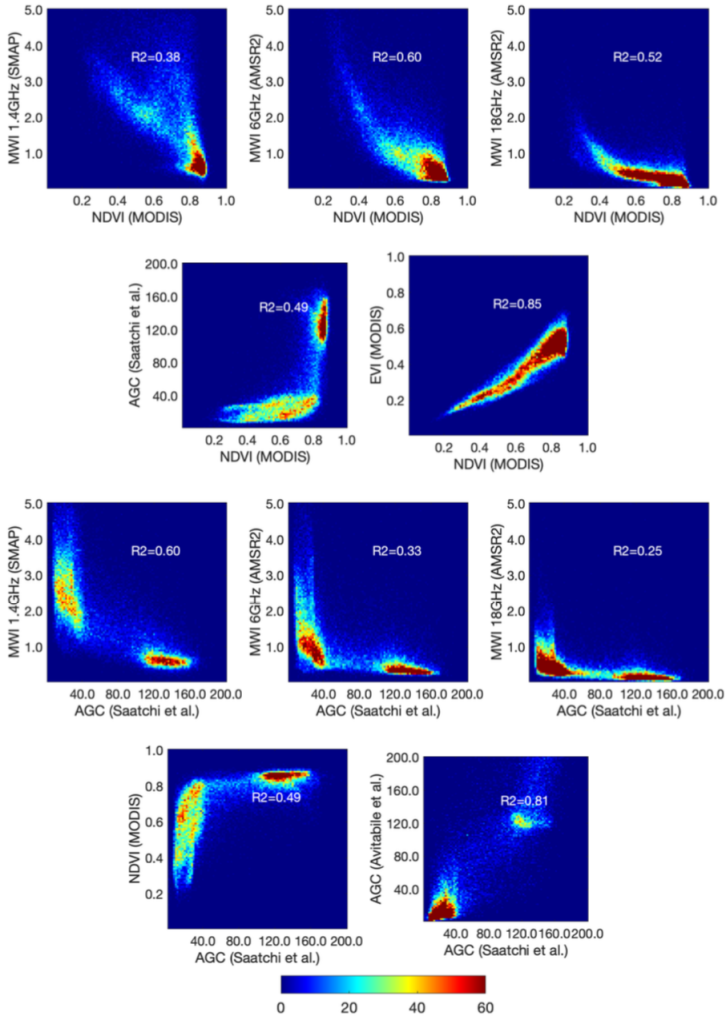

Figure 2: Density plots of MWI at 1.4, 6, and 18 GHz and vegetation related variables (NDVI, EVI, and AGC), calculated over the Tropics, for June 2015, as a function of NDVI (MODIS) for the two top rows, and as a function of AGC [Saatchi et al., 2011] for the two bottom rows. The colors indicate the number of pixels per bin. The coefficient of determination (R^2) is indicated. Deserts and surface water pixels are excluded from the statistics.

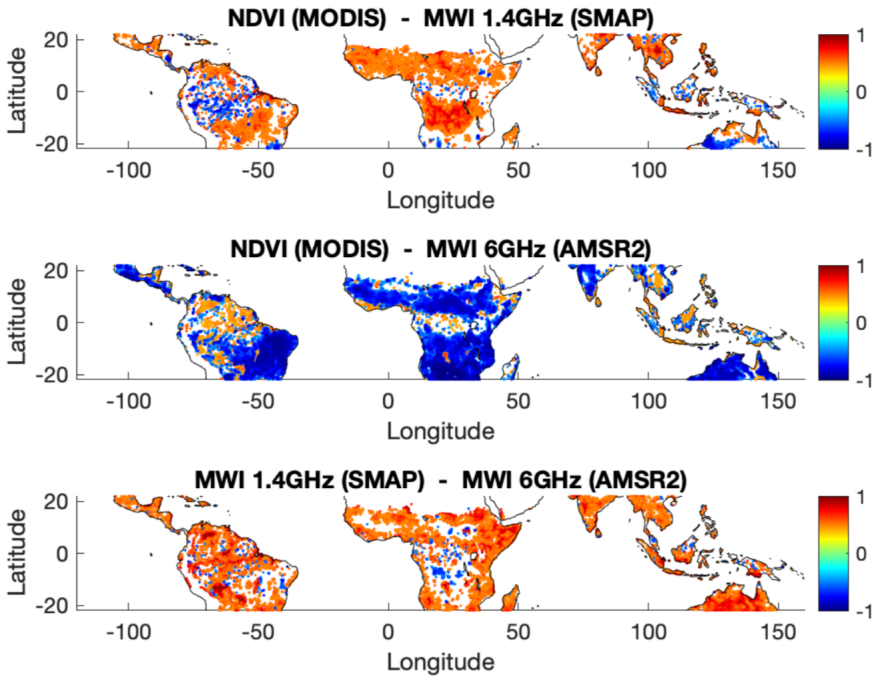

Figure 3: Maps of the temporal correlations over the Tropics between NDVI (MODIS) and MWI at 1.4 GHz (SMAP) (top panel), between NDVI (MODIS) and MWI at 6 GHz (AMSR2) (middle panel), and between MWI at 1.4 GHz (SMAP) and at 6 GHz (AMSR2) (bottom panel). Pixels with p-values below 0.05 are not displayed.

structure (trunk, branches, leaves), with their respective constituents and sizes. Except over dense forests, with increasing NDVI (due to vegetation chlorophyll activity or 'greenness'), the emissivity polarization difference at 6 GHz (and at higher frequencies) decreases with increasing extinction in the foliage. At 1.4 GHz, the vegetation extinction is lower than at higher frequencies: the effect of the soil moisture on the variability of the emissivity polarization difference can still be observed when the vegetation is not totally opaque.

Figure 4 presents cross-sections of MWI, NDVI, and AGC at two longitudes in Africa and in South America, for June and December. All the variables are normalized for an easier comparison (see the figure caption). Large gradients are observed for all variables in Africa, from the semi-arid

regions north of 5°N, to the dense forest around the equator, down to the shrubland and grassland southwards. In South America, the Amazon River and its associated floodplains induce very large values of MWIs (at $\sim$ 3°S at 60°W and $\sim$ 2°S at 55°W). The presence of standing water at the surface generates strong polarization differences in the microwave surface emissivity and this property has been exploited to derive the extent and dynamics of the surface water at global scale (e.g., [Prigent et al., 2020]). In the equatorial forest where AGC reaches its maximum values, in Africa as well as in South America, NDVI reaches high values whereas MWIs show their lowest values, as expected. Note that in these evergreen tropical forests, NDVI tends to vary during the year, although MWI values appear quite stable, regardless of the season. These temporal changes in NDVI over evergreen forests have already been documented at several occasions (e.g., [Prigent et al., 2001]) and are essentially related to atmospheric contamination (water vapor and possibly clouds) in NDVI, with the contamination modulated by the displacement of the Inter Tropical Convective Zone with seasons. Over shrubland and grassland with low AGC, NDVI during summer can reach values of the same order as over very dense forests (see for instance the high values of NDVI in Africa in December around 10°S). In these regions, the seasonal changes of MWI at 1.4 GHz is significant and much larger than at higher frequencies, with even opposite behavior as observed between 5°S and 10°S at longitude 25°E (top right panel in Figure 4). An increase in soil moisture between June and December induces a vegetation increase (as indicated by the increase in NDVI). It results in an increase in the emissivity polarization difference (MWI) at 1.4 GHz, very sensitive to the soil moisture and not significantly attenuated by the vegetation, whereas at higher microwave frequencies, MWI decreases for increasing vegetation extinction. Depending on the vegetation parameters at a given time of the year and depending on the wavelength of observation, the soil and vegetation contribute differently to the signal, and these complementarities can be exploited to better characterize the vegetation with multi-frequency passive microwaves.

For selected vegetation types in Africa (following the GlobCover classification), Figure 5 presents the normalized histograms of NDVI and MWIs at 1.4, 6, 18 GHz for June and December, for two regions north and south of the equator. For each region and each vegetation type, the mean AGC [Saatchi et al., 2011] is indicated. For a given season, with increasing vegetation density from grassland to evergreen forest (and corresponding AGC increase), NDVI increases and MWIs tend to decrease, as expected. The temporal changes from June to December for a given vegetation type is more complex, as already observed in Figure 3 with positive or negative tempo-

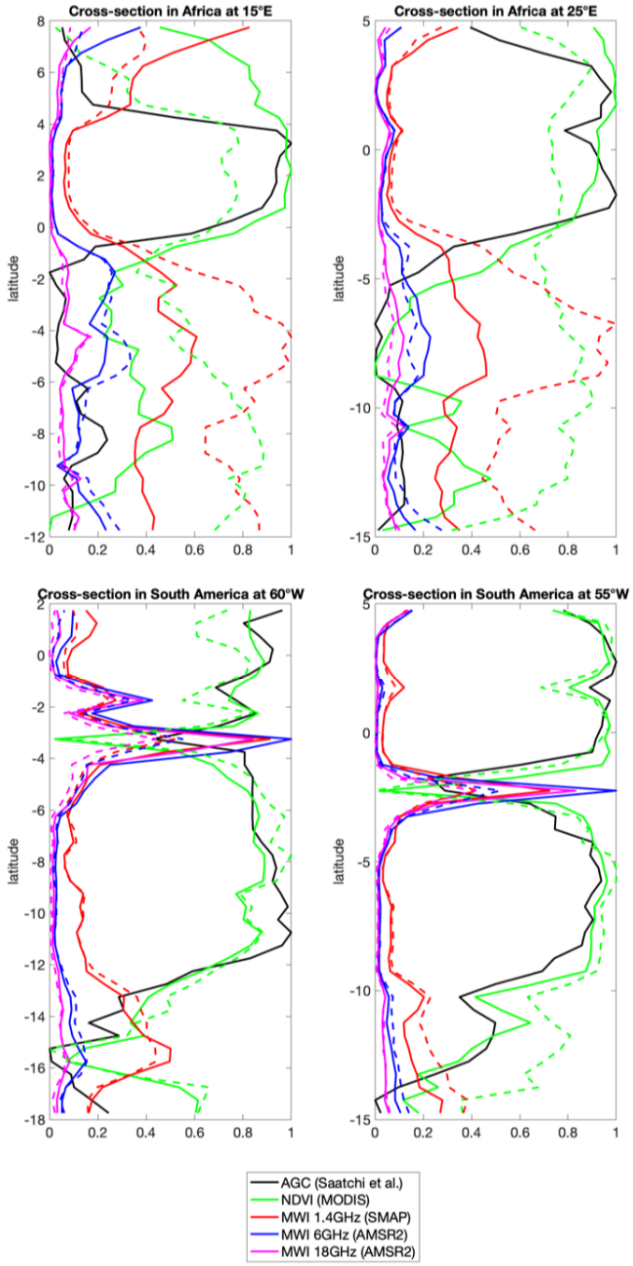

Figure 4: Cross-sections of AGC [Saatchi et al., 2011], NDVI (MODIS), MWI at 1.4 GHz (SMAP), and MWI at 6 and 36 GHz (AMSR2), for two different longitudes in Africa (top), and in South America (bottom), for two months (June as solid lines and December as dashed lines). Data are averaged over 2° around the given longitude, and over the month for the dynamic variables. For each figure separately, AGC, NDVI, and MWIs are normalized by their maximum and minimum values over the two months (and over the three frequencies for MWIs).

ral correlations between NDVI and MWIs, depending on the frequency and on the relative contribution of the soil and vegetation in the signal. The evergreen forest has stable signatures for both seasons and regions, for all variables except some changes for NDVI as already discussed.

4.2 Retrieval of the vegetation parameters and quantification of microwave observation synergy

So far, we analyzed the individual sensitivity of each passive microwave observation from 1.4 to 36 GHz to the vegetation parameters, through the use of a simple microwave index. Recently, several papers also studied the individual sensitivity of the VOD in the different frequency bands to the vegetation information (e.g., AGC in [Chaparro et al., 2019] or the vegetation height in [Baur et al., 2019]).

Now, we propose to evaluate the synergy of the multi-frequency microwave observations by comparing the retrieval of NDVI and AGC, using different microwave frequency combinations. The analysis in the previous section showed that the spatial and temporal correlation patterns between MWIs and vegetation information (NDVI and AGC) could be rather complex and not necessarily linear, justifying the use of the NN retrieval method, compared to multi-linear regressions.

Tests are conducted, first using individual passive microwave frequencies to reproduce the vegetation information, second using their different combinations to analyze their synergy, including the combination that corresponds to CIMR. Ten different passive microwave combinations have been tested: first, each frequency separately (the 1.4 GHz alone corresponding to SMAP), then the 6, 10, 18, and 36 GHz combination corresponding to AMSR2, and finally the successive addition of frequencies to the 1.4 GHz, to reach the full combination of considered frequencies corresponding to the CIMR configuration. For each frequency, the MWI and the TBH are both used as inputs to the NNs. For each vegetation parameter and frequency combination, a new NN is trained: 20 NNs were thus trained, 10 for the NDVI retrieval and 10 for the AGC retrieval.

All NNs are trained on the same NDVI or AGC training dataset, for comparison purposes between the frequency combinations. The training dataset contains $\sim$140 000 combinations of the vegetation parameter and the passive microwave observations, for NDVI and AGB separately. For NDVI, time coincident NDVI and passive microwave observations are considered as previously mentioned. For AGC, the NN to reproduce AGC is trained on the same AGC values, regardless of the time period but we tested the train-

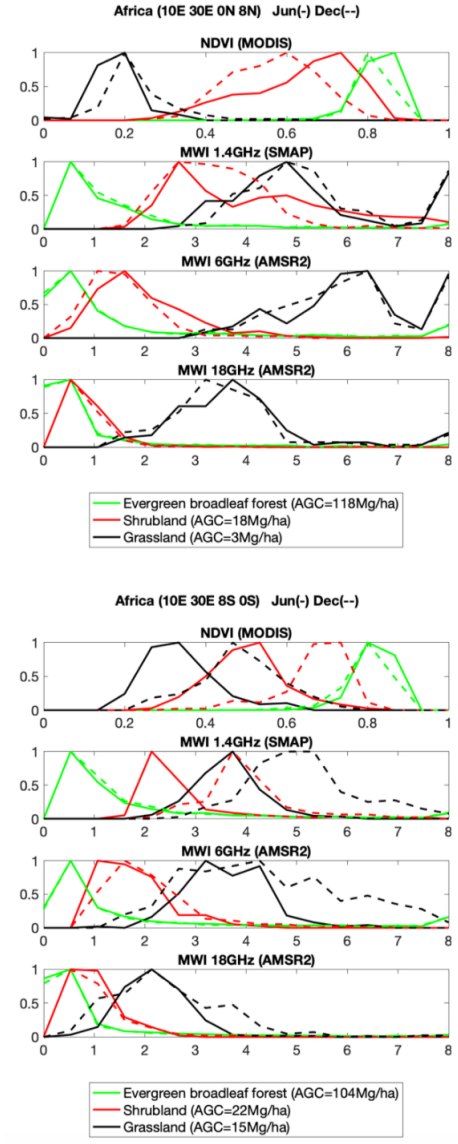

Figure 5: Normalized histograms of NDVI and MWIs at 1.4, 6, and 18 GHz, for two regions in Africa, for selected vegetation types, as described by the GlobCover classification, for June (solid lines) and December (dashed lines). Top: north of the equator. Bottom: south of the equator. For each region and each vegetation type, the mean AGC from [Saatchi et al., 2011] is indicated.

ing of AGC retrieval by first averaging the microwave observations at the different time steps, and very similar results were obtained. The natural distribution of AGC shows two distinct peaks, one for low AGC at ∼30 Mg/ha and another one at high AGC at ∼120 Mg/ha (see Figure 2). The original training database distribution is resampled to avoid an under representation of medium AGC values. This procedure has already been applied with success at different occasions for similar problems (e.g., [Prigent et al., 2020]) and it has been systematically applied to the training of all the frequency combinations for the retrieval of AGC. NDVI distribution is smoother and this procedure has not been applied to the retrieval of this variable.

Figure 6 presents the results of the retrieval evaluation for both NDVI and AGC, for all the passive microwave combinations, as evaluated with the two selected metrics, the coefficient of determination R^2, and the $RMSE$. The evaluation is performed on the remaining 8-day periods in the original dataset, excluding the four 8-day periods from the training dataset.

For the retrieval of NDVI, none of the frequency alone matches the performances obtained with the combination of at least two frequencies. 1.4 and 10 GHz, when used alone, tend to produce the best results. Note that the linear correlation of MWI at 1.4 GHz with NDVI was lower than at higher frequencies (see Figure 2). We checked that when using a multi-linear regression retrieval with the same inputs (MWI and TBH for each frequency), the retrieval results were poorer at 1.4 GHz than at higher frequencies (and significantly much poorer than with the NN for each frequency). The NN retrieval systematically outperforms the linear regression and manages to extract the complex non-linear information present in the observations. The coefficient of determination R^2 between retrieved and true NDVI reaches 0.84 when using all CIMR frequencies, with a RMSE of 0.07 (compared to 0.09 with the 1.4 GHz only). Compared to AMSR2, the CIMR frequency combination performs slightly better with respect to the two selected metrics for NDVI, but the improvement is not significant, especially when considering that the addition of 1.4 GHz to the frequencies from 6 to 36 GHz penalizes the spatial resolution of the retrieved product (with a spatial resolution of 55 km at 1.4 GHz compared to 15 km at 6 GHz with CIMR).

For the retrieval of AGC, 1.4 GHz is the frequency that has the highest information content, with significantly better performances than any other frequency alone. The coefficient of determination R^2 drops significantly from 1.4 to 6 GHz and gets worse at higher frequencies (Figure 6, top panel). That was already concluded by other studies analyzing the relationship between AGC and the VODs for the different frequencies (e.g., [Chaparro et al., 2019]). In parallel, AGC retrieval error shows a sharp

increase from 1.4 to 6 GHz and then a moderate increase for the higher frequencies. The addition of the higher frequencies to the 1.4 GHz channels improves the AGC retrieval results, with R^2 reaching 0.82 with CIMR (compared to 0.77 with SMAP 1.4 GHz alone), with a RMSE of 21 Ma/ha (compared to 24 Ma/ha with 1.4 GHz only).

Figure 7 shows the RMSE of the retrievals for each vegetation variable, as a function of the variable itself, for the SMAP, AMSR2, and CIMR configurations. For NDVI, CIMR and AMSR2 performances are close, regardless of the NDVI values. For AGC, CIMR performances closely follow the variations of the SMAP ones, as a function of AGC. However, from low to high NDVI or AGC, the CIMR frequency combination always provides the lowest error for both NDVI and AGC estimations. It is thus expected that CIMR will contribute to an improved and consistent estimation of both photosynthetic and non-photosynthetic above ground biomass.

A similar exercice has been applied to EVI (instead of NDVI) and to AGC estimated by [Avitabile et al., 2016] (instead of AGC from [Saatchi et al., 2011]). For these two variables, the performance of the retrievals is reduced, compared to NDVI and AGC from [Saatchi et al., 2011] (not shown). This is especially noticeable for EVI, regardless of the frequency combination. It could be interpreted as a reduced consistency between the passive microwave observations and EVI and AGC from [Avitabile et al., 2016], compared to what is existing with NDVI and AGC from [Saatchi et al., 2011]. [Fan et al., 2019] also tends to favor AGC from [Saatchi et al., 2011] compared to the one from [Avitabile et al., 2016] for comparison with VOD at 1.4 GHz. The saturation observed with EVI over the tropical forests, as compared to NDVI, can be responsible for the reduced performances of the EVI retrieval.

5 Conclusion

Satellite passive microwave observations from 1.4 to 36 GHz already showed sensitivity to vegetation parameters, primarily through the calculations of VODs at each frequency separately. Here we evaluated the synergy of this frequency range for vegetation characterization through the estimation of two vegetation parameters, the foliage photosynthesis activity as represented by NDVI, and the vegetation above ground carbon stock with AGC, using different combinations of channels in the considered frequency range. NN retrievals are trained on the two considered vegetation parameters, for several microwave channel combinations, including the CIMR configuration.

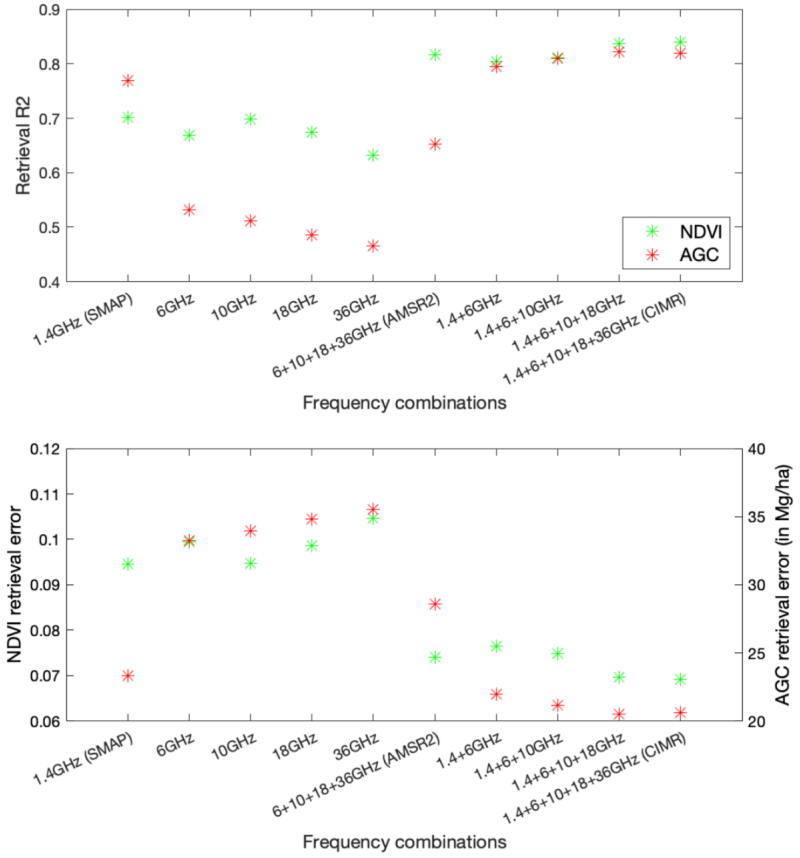

Figure 6: Performance of NDVI and AGC retrievals with different passive microwave combinations. True NDVI and AGC are respectively from MODIS and from [Saatchi et al., 2011]. Top: the coefficient of determination R^2 between the retrieval and the truth for NDVI (left axis) and AGC (right axis). Bottom: the retrieval error (RMSE) for NDVI (left axis) and AGC (right axis).

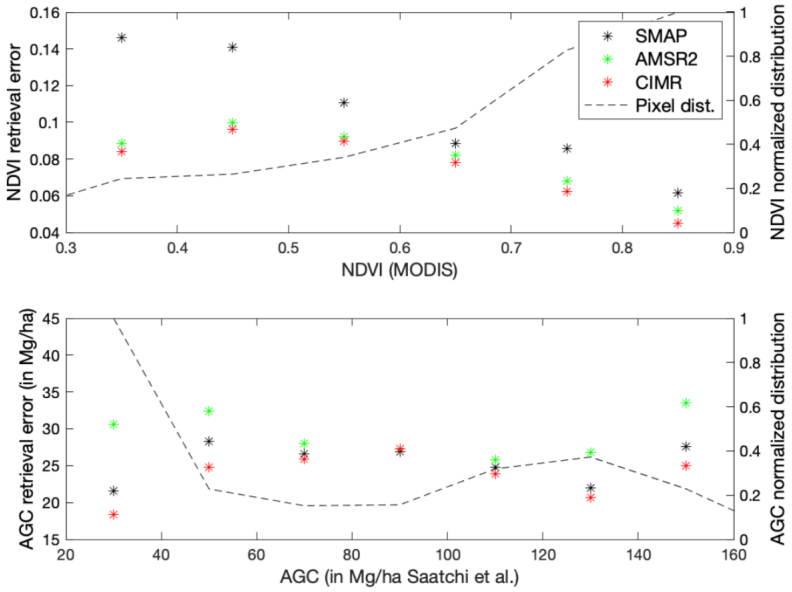

Figure 7: Top: NDVI retrieval error (RMSE), as a function of NDVI, for SMAP, AMSR2, and CIMR frequency combinations. The normalized NDVI distribution is also indicated in dashed line (see left axis). Bottom: Same for AGC.

This methodology avoids the use of any assumptions in the complex interaction between the surface (vegetation and soil) and the radiation, as well as any ancillary observations, to propose a genuine and objective evaluation of the information content of the passive microwave frequencies for vegetation characterization, without any a priori.

The performance of the NN vegetation retrievals is used to quantify the synergy of different frequency combinations. For the retrieval of NDVI, the coefficient of determination R^2 between retrieved and true NDVI reaches 0.84 when using the full 1.4 to 36 GHz range as will be measured by CIMR, with a retrieval error of 0.07. For the retrieval of AGC, the coefficient of determination R^2 reaches 0.82 with CIMR, with an error of 21 Mg/ha. This study also confirmed that 1.4 GHz observations have the highest sensitivity to AGC, as compared to other frequencies up to 36 GHz, at least under tropical environments.

CIMR will provide valuable ecological indicators to enhance our present global vegetation understanding. Considering both vegetation aspects together (foliage photosynthesis activity and carbon stocks) offers a more robust and consistent characterization and assessment of long-term vegetation dynamics at large scale.

Acknowledgements

The authors would like to thank Jean-Pierre Wigneron for valuable discussions. They would also like to thank Craig Donlon and the ESA CIMR Mission Advisory Group. Comments from the editor and from three anonymous reviewers made it possible to significantly improve the initial manuscript.

References

[Aires et al., 2001] Aires, F., Prigent, C., Rossow, W., and Rothstein, M. (2001). A new neural network approach including first guess for retrieval of atmospheric water vapor, cloud liquid water path, surface temperature, and emissivities over land from satellite microwave observations. *Journal of Geophysical Research: Atmospheres*, 106(D14):14887–14907.

[Aires et al., 2005] Aires, F., Prigent, C., and Rossow, W. B. (2005). Sensitivity of satellite microwave and infrared observations to soil moisture at a global scale: 2. Global statistical relationships. *Journal of Geophysical Research D: Atmospheres*, 110(11):1–14.

[Avitabile et al., 2016] Avitabile, V., Herold, M., Heuvelink, G. B., Lewis, S. L., Phillips, O. L., Asner, G. P., Armston, J., Ashton, P. S., Banin, L., Bayol, N., et al. (2016). An integrated pan-tropical biomass map using multiple reference datasets. *Global change biology*, 22(4):1406–1420.

[Baccini et al., 2012] Baccini, A., Goetz, S., Walker, W., Laporte, N., Sun, M., Sulla-Menashe, D., Hackler, J., Beck, P., Dubayah, R., Friedl, M., et al. (2012). Estimated carbon dioxide emissions from tropical deforestation improved by carbon-density maps. *Nature climate change*, 2(3):182–185.

[Baur et al., 2019] Baur, M. J., Jagdhuber, T., Feldman, A. F., Akbar, R., and Entekhabi, D. (2019). Estimation of relative canopy absorption and scattering at l-, c-and x-bands. *Remote Sensing of Environment*, 233:111384.

[Bernard et al., 1990] Bernard, R., Hallikainen, M., Kerr, Y., Kuenzi, K., Maetzler, C., Pampaloni, P., Duchossois, G., Menard, Y., and Rast, M. (1990). Mimr: Multifrequency passive microwave radiometer. Technical report.

[Bonan, 2015] Bonan, G. (2015). *Ecological climatology: concepts and applications*. Cambridge University Press.

[Brandt et al., 2018] Brandt, M., Wigneron, J.-P., Chave, J., Tagesson, T., Penuelas, J., Ciais, P., Rasmussen, K., Tian, F., Mbow, C., Al-Yaari, A., et al. (2018). Satellite passive microwaves reveal recent climate-induced carbon losses in african drylands. *Nature ecology & evolution*, 2(5):827–835.

[Brown and Lugo, 1982] Brown, S. and Lugo, A. E. (1982). The storage and production of organic matter in tropical forests and their role in the global carbon cycle. *Biotropica*, pages 161–187.

[Calvet et al., 2010] Calvet, J.-C., Wigneron, J.-P., Walker, J., Karbou, F., Chanzy, A., and Albergel, C. (2010). Sensitivity of passive microwave observations to soil moisture and vegetation water content: L-band to w-band. *IEEE Transactions on geoscience and remote sensing*, 49(4):1190–1199.

[Chaparro et al., 2019] Chaparro, D., Duveiller, G., Piles, M., Cescatti, A., Vall-Llossera, M., Camps, A., and Entekhabi, D. (2019). Sensitivity of l-band vegetation optical depth to carbon stocks in tropical forests: a

comparison to higher frequencies and optical indices. *Remote Sensing of Environment*, 232:111303.

[Choudhury et al., 1987] Choudhury, B., Tucker, C., Golus, R., and Newcomb, W. (1987). Monitoring vegetation using nimbus-7 scanning multichannel microwave radiometer's data. *International Journal of Remote Sensing*, 8(3):533–538.

[Chukhlantsev, 2006] Chukhlantsev, A. A. (2006). *Microwave radiometry of vegetation canopies*, volume 24. Springer Science & Business Media.

[de Rosnay et al., 2020] de Rosnay, P., Munoz-Sabater, J., Albergel, C., Isaksen, L., English, S., Drusch, M., and Wigneron, J.-P. (2020). Smos brightness temperature forward modelling and long term monitoring at ecmwf. *Remote Sensing of Environment*, 237:111424.

[Elias and Potvin, 2003] Elias, M. and Potvin, C. (2003). Assessing inter- and intra-specific variation in trunk carbon concentration for 32 neotropical tree species. *Canadian Journal of Forest Research*, 33(6):1039–1045.

[Entekhabi et al., 2014] Entekhabi, D., Yueh, S., and De Lannoy, G. (2014). Smap handbook.

[Fan et al., 2019] Fan, L., Wigneron, J.-P., Ciais, P., Chave, J., Brandt, M., Fensholt, R., Saatchi, S. S., Bastos, A., Al-Yaari, A., Hufkens, K., et al. (2019). Satellite-observed pantropical carbon dynamics. *Nature plants*, 5(9):944–951.

[Fernandez-Moran et al., 2017] Fernandez-Moran, R., Wigneron, J.-P., De Lannoy, G., Lopez-Baeza, E., Parrens, M., Mialon, A., Mahmoodi, A., Al-Yaari, A., Bircher, S., Al Bitar, A., et al. (2017). A new calibration of the effective scattering albedo and soil roughness parameters in the smos sm retrieval algorithm. *International journal of applied earth observation and geoinformation*, 62:27–38.

[Ferrazzoli et al., 2002] Ferrazzoli, P., Guerriero, L., and Wigneron, J.-P. (2002). Simulating l-band emission of forests in view of future satellite applications. *IEEE Transactions on Geoscience and Remote Sensing*, 40(12):2700–2708.

[Frappart et al., 2020] Frappart, F., Wigneron, J.-P., Li, X., Liu, X., Al-Yaari, A., Fan, L., Wang, M., Moisy, C., Le Masson, E., Lafkih, Z. A., et al. (2020). Global monitoring of the vegetation dynamics from the vegetation optical depth (vod): A review. *Remote Sensing*, 12(18):2915.

[Hagan and Menhaj, 1994] Hagan, M. T. and Menhaj, M. B. (1994). Training feedforward networks with the marquardt algorithm. *IEEE transactions on Neural Networks*, 5(6):989–993.

[Huete et al., 2002] Huete, A., Didan, K., Miura, T., Rodriguez, E. P., Gao, X., and Ferreira, L. G. (2002). Overview of the radiometric and biophysical performance of the modis vegetation indices. *Remote sensing of environment*, 83(1-2):195–213.

[Jimenez et al., 2009] Jimenez, C., Prigent, C., and Aires, F. (2009). Toward an estimation of global land surface heat fluxes from multisatellite observations. *Journal of Geophysical Research: Atmospheres*, 114(D6).

[Jones et al., 2011] Jones, M. O., Jones, L. A., Kimball, J. S., and McDonald, K. C. (2011). Satellite passive microwave remote sensing for monitoring global land surface phenology. *Remote Sensing of Environment*, 115(4):1102–1114.

[Jones et al., 2014] Jones, M. O., Kimball, J. S., and Nemani, R. R. (2014). Asynchronous amazon forest canopy phenology indicates adaptation to both water and light availability. *Environmental Research Letters*, 9(12):124021.

[Kilic et al., 2018] Kilic, L., Prigent, C., Aires, F., Boutin, J., Heygster, G., Tonboe, R. T., Roquet, H., Jimenez, C., and Donlon, C. (2018). Expected performances of the copernicus imaging microwave radiometer (cimr) for an all-weather and high spatial resolution estimation of ocean and sea ice parameters. *Journal of Geophysical Research: Oceans*, 123(10):7564–7580.

[Kolassa et al., 2013] Kolassa, J., Aires, F., Polcher, J., Prigent, C., Jimenez, C., and Pereira, J.-M. (2013). Soil moisture retrieval from multi-instrument observations: Information content analysis and retrieval methodology. *Journal of Geophysical Research: Atmospheres*, 118(10):4847–4859.

[Konings et al., 2016] Konings, A. G., Piles, M., Rotzer, K., McColl, K. A., Chan, S. K., and Entekhabi, D. (2016). Vegetation optical depth and scattering albedo retrieval using time series of dual-polarized l-band radiometer observations. *Remote Sensing of Environment*, 172:178–189.

[Li et al., 2021] Li, X., Wigneron, J.-P., Frappart, F., Fan, L., Ciais, P., Fensholt, R., Entekhabi, D., Brandt, M., Konings, A. G., Liu, X., et al.

(2021). Global-scale assessment and inter-comparison of recently developed/reprocessed microwave satellite vegetation optical depth products. *Remote Sensing of Environment*, 253:112208.

[Liu et al., 2011] Liu, Y. Y., de Jeu, R. A., McCabe, M. F., Evans, J. P., and van Dijk, A. I. (2011). Global long-term passive microwave satellite-based retrievals of vegetation optical depth. *Geophysical Research Letters*, 38(18).

[Maeda et al., 2016] Maeda, T., Taniguchi, Y., and Imaoka, K. (2016). Gcom-w1 amsr2 level 1r product: Dataset of brightness temperature modified using the antenna pattern matching technique. *IEEE Transactions on Geoscience and Remote Sensing*, 54(2):770–782.

[Momen et al., 2017] Momen, M., Wood, J. D., Novick, K. A., Pangle, R., Pockman, W. T., McDowell, N. G., and Konings, A. G. (2017). Interacting effects of leaf water potential and biomass on vegetation optical depth. *Journal of Geophysical Research: Biogeosciences*, 122(11):3031–3046.

[Njoku and Li, 1999] Njoku, E. G. and Li, L. (1999). Retrieval of land surface parameters using passive microwave measurements at 6-18 ghz. *IEEE Transactions on Geoscience and Remote Sensing*, 37(1):79–93.

[Owe et al., 2001] Owe, M., de Jeu, R., and Walker, J. (2001). A methodology for surface soil moisture and vegetation optical depth retrieval using the microwave polarization difference index. *IEEE Transactions on Geoscience and Remote Sensing*, 39(8):1643–1654.

[Paloscia and Pampaloni, 1988] Paloscia, S. and Pampaloni, P. (1988). Microwave polarization index for monitoring vegetation growth. *IEEE Transactions on Geoscience and Remote Sensing*, 26(5):617–621.

[Piepmeier et al., 2018] Piepmeier, J., Mohammed, P., Peng, J., Kim, E., De Amici, G., and Ruf, C. (2018). Smap l1b radiometer half-orbit time-ordered brightness temperatures. Technical report.

[Prigent et al., 2001] Prigent, C., Aires, F., Rossow, W., and Matthews, E. (2001). Joint characterization of vegetation by satellite observations from visible to microwave wavelengths: A sensitivity analysis. *Journal of Geophysical Research: Atmospheres*, 106(D18):20665–20685.

[Prigent et al., 2020] Prigent, C., Jimenez, C., and Bousquet, P. (2020). Satellite-derived global surface water extent and dynamics over the last

25 years (giems-2). *Journal of Geophysical Research: Atmospheres*, 125(3):e2019JD030711.

[Rodriguez-Fernandez et al., 2019] Rodriguez-Fernandez, N., de Rosnay, P., Albergel, C., Richaume, P., Aires, F., Prigent, C., and Kerr, Y. (2019). Smos neural network soil moisture data assimilation in a land surface model and atmospheric impact. *Remote Sensing*, 11(11):1334.

[Rumelhart et al., 1986] Rumelhart, D. E., Hinton, G. E., and Williams, R. J. (1986). Learning internal representations by error propagation. In Rumelhart, D. E., McClelland, J. L., and the PDP Research Group, editors, *Parallel distributed processing: explorations in the microstructure of cognition, vol. I,*, pages 318–362. MIT Press, Cambridge, Mass.

[Saatchi et al., 2011] Saatchi, S. S., Harris, N. L., Brown, S., Lefsky, M., Mitchard, E. T., Salas, W., Zutta, B. R., Buermann, W., Lewis, S. L., Hagen, S., et al. (2011). Benchmark map of forest carbon stocks in tropical regions across three continents. *Proceedings of the national academy of sciences*, 108(24):9899–9904.

[Shi et al., 2008] Shi, J., Jackson, T., Tao, J., Du, J., Bindlish, R., Lu, L., and Chen, K. (2008). Microwave vegetation indices for short vegetation covers from satellite passive microwave sensor amsr-e. *Remote sensing of environment*, 112(12):4285–4300.

[Tucker, 1979] Tucker, C. J. (1979). Red and photographic infrared linear combinations for monitoring vegetation. *Remote sensing of environment*, 8:127–150.

[Ulaby and Long, 2015] Ulaby, F. and Long, D. (2015). *Microwave radar and radiometric remote sensing*. Artech House.

[Ulaby et al., 1981] Ulaby, F. T., Moore, R. K., and Fung, A. K. (1981). Microwave remote sensing: Active and passive. volume 1-microwave remote sensing fundamentals and radiometry.

[Wigneron et al., 1995] Wigneron, J.-P., Chanzy, A., Calvet, J.-C., and Bruguier, N. (1995). A simple algorithm to retrieve soil moisture and vegetation biomass using passive microwave measurements over crop fields. *Remote Sensing of Environment*, 51(3):331–341.

[Wigneron et al., 2007] Wigneron, J.-P., Kerr, Y., Waldteufel, P., Saleh, K., Escorihuela, M.-J., Richaume, P., Ferrazzoli, P., De Rosnay, P., Gurney,

R., Calvet, J.-C., et al. (2007). L-band microwave emission of the biosphere (l-meb) model: Description and calibration against experimental data sets over crop fields. *Remote Sensing of Environment*, 107(4):639–655.

[Wigneron et al., 2021] Wigneron, J.-P., Li, X., Frappart, F., Fan, L., Al-Yaari, A., De Lannoy, G., Liu, X., Wang, M., Le Masson, E., and Moisy, C. (2021). Smos-ic data record of soil moisture and l-vod: Historical development, applications and perspectives. *Remote Sensing of Environment*, 254:112238.